Dependence of *N*-Nitrosodimethylamine Photodecomposition on the Irradiation Wavelength: Excitation to the S_2 State as a Doorway to the Dimethylamine Radical Ground-State Chemistry

Daniel Peláez,* Juan F. Arenas, Juan C. Otero, and Juan Soto*

Department of Physical Chemistry, Faculty of Sciences, University of Málaga, E-29071 Málaga, Spain

dpr@uma.es; soto@uma.es

Received February 27, 2007

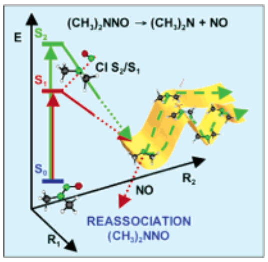

The photochemistry of *N*-nitrosodimethylamine after excitation to the S_1 and S_2 states has been studied with the complete active space self-consistent field method (CASSCF) and the second-order multiconfigurational perturbation theory (CASPT2). The calculated vertical transitions agree with the experiment: the $S_0 \rightarrow S_1$ transition occurs at 3.29 eV ($f = 0.003$ au), the $S_0 \rightarrow S_2$ transition at 5.30 eV ($f = 0.17$ au) and the first excited triplet state is computed at 2.48 eV. Solvent effects have been reproduced by means of PCM calculations. It is shown that excitation to S_1 and S_2 yields the same photoproducts: $(CH_3)_2N$ (1^2B_1) and NO ($X^2\Pi$). However, while on S_1 the process is adiabatic, the process on S_2 implies an ultrafast decay through a planar S_2/S_1 conical intersection. Our calculations are consistent with the reversibility of the N−N dissociation after irradiation at 363.5 nm and the observed dimethylamine radical reactions when irradiated at 248 nm, namely, H extrusion, a one-step process (41.3 kcal/mol), and methyl radical extrusion, a two-step process (44.0 kcal/mol and 31.5 kcal/mol). Finally, two more aspects are considered: (i) the topology of the T_1 surface where two minima have been found to correlate with the phosphorescence emission band and (ii) the influence of tautomerizations which is shown to be neglectable.

I. Introduction

Although described more than a hundred years ago,[1] nitrosamines have not deserved much attention until the mid-fifties of the last century when Magee and Barnes reported the carcinogenic character of *N*-nitrosodimethylamine,[2] (NDMA). Since then, nitrosamines have been shown to be ubiquitous, they have been found in food,[3] tobacco smoke,[4] and even in drinking water.[5,6] In this respect, strong efforts are made to find an effective way of removing such a compound from water photochemically;[5] however, no unified picture of the decomposition mechanism has been established up to date.[5] The ubiquity of NDMA, particularly in vivo, occurs because of the facile N−N bond formation owing to easy access to precursors, such as amines and nitrosating agents generated from either endogenous NO[7] or nitrite salts, which are traditionally employed as preservatives in food industry. Recently, the World Health Organization has published an extensive report on NDMA.[8]

---

(1) Fischer, E. *Annalen* **1879**, *199*, 299.

(2) Magee, P. N.; Barnes, J. M. *Brit. J. Cancer* **1956**, *10*, 114.

(3) (a) Masuda, S.; Uchida, S.; Terashima, Y.; Kuramoto, H.; Serizawa, V.; Deguchi, Y.; Yanai, K.; Sugiyama, C.; Oguni, I.; Kinae, N. *J. Health Sci.* **2006**, *52*, 211. (b) Larsson, S. C.; Bergkvist, L.; Wolk, A. *Int. J. Cancer* **2006**, *119*, 915. (c) Okafor, P. N.; Nwogbo, E. *Afr. J. Biotechnol.* **2005**, *4*, 1105.

(4) Lao, Y. B.; Villalta, P. W.; Wang, M. Y.; Cheng G, G.; Sturla, S. J. *Abstr. Pap. Am. Chem. Soc.* **2005**, *230*, U1847−39-TOXI.

(5) (a) Lee, C.; Choi, W.; Kim, Y. G.; Yoon, J. *Environ. Sci. Technol.* **2005**, *39*, 2101. (b) Schreiber, I. M.; Mitch, W. A. *Environ. Sci. Technol.* **2006**, *40*, 6007.

(6) (a) Najm, I.; Trussel, R. R. J. *Am. Water Works Assoc.* **2001**, (*Feb*). (b) Sen, N. P.; Seaman, S. W.; Brousseau, R. *J. Agric. Food Chem.* **1996**, *44*, 1498.

(7) Wink, D. A.; Vodovotz, Y.; Laval, J.; Laval, F.; Dewhirst, M. W.; Mitchell, J. B. *Carcinogenesis* **1998**, *19* (5), 711.

10.1021/jo070399a CCC: \$37.00 © 2007 American Chemical Society
Published on Web 05/22/2007

From the environmental point of view, nitrosamines have attracted much interest as intermediates in the elimination of nitrogen oxides with amino radicals in atmospheric processes, as well as in combustion ones.[9,10] Additionally, their electronic structure has been the subject of study because nitrosamines present an electron donating group ($(CH_3)_2N$) directly linked to an electron withdrawing group (NO).[11]

Our interest in this molecule lies in the fact that nitrosamines are photoproducts of their respective nitramines. This has been proven both experimentally[9b,11] and theoretically.[12] We, ourselves, have shown the possibility of direct generation of the nitroso derivative after the internal conversion S_3/S_2 in nitromethane and nitramide.[12]

Thermally, NDMA has been shown to exhibit a main reaction channel: scission of the weak N−N bond to yield $(CH_3)_2N$ and NO.[9] Lazarou et al. studied by means of the very low-pressure reactor (VLPR) technique, the reaction rates of $(CH_3)_2N$ and NO and $(CH_3)_2N$ and NO_2 associations. They found that the former process is eight times slower than the latter one, and by using the conventional transition state theory they proposed that both reactions proceed through a loose transition state with an internuclear N−N distance of 2.5 Å. On the other hand, Nigenda et al. by pulsed laser pyrolysis determined that, at the experimental conditions (temperature range 870−990 K), the decomposition of NDMA led to the irreversible formation of imine (CH_3NCH_2) by loss of hydrogen in the presence of a scavenger.

With respect to the photochemistry of NDMA, it must be noted that the formation of aminium radicals is the main reaction in solution, while in the gas-phase the N−N bond breaking constitutes the initial and main process. The reactivity of NDMA in solution has been extensively studied by Chow et al.[13] who reported the possibility of direct excitation of NDMA to the first triplet state at 2.73 eV.[13a]

Geiger et al.[14] obtained the gas-phase UV absorption spectrum of NDMA. It exhibits a weak band, between 24 500 and 30 000 cm^{-1}, with a maximum at 27 500 cm^{-1} (363.5 nm) presenting a vibrational progression with an oscillator strength of 0.009 and an unstructured strong band centered at 44 000 cm^{-1} (227 nm) with an oscillator strength of 0.12. They also studied the reactions following excitation at 363.5 nm, which corresponds to the $S_0 \rightarrow S_1$ transition, and at 248 nm, corresponding to the $S_0 \rightarrow S_2$ transition. The former was shown, by isotopic exchange with ^{15}NO, to lead exclusively to N−N bond breaking with a quantum yield of unity, a fraction of the NO fragment being in an excited vibrational state. Since NDMA was newly reformed after dissociation, they estimated a very long lifetime for the dimethyl amino radical ($t > 0.5$ s). Nevertheless, excitation at 248 nm implies a different mechanism since it gives rise to a wide manifold of products, namely, *N*-methylidene-methylamine (CH_3NCH_2), its trimer, formaldoxime (CH_2NOH), NO, H_2, N_2, N_2O, and small amounts of ethane. The first step involves N−N bond breaking; in addition, Geiger et al.[14] propose that this process should be followed by any of the secondary reactions of the amine radical:

$$(CH_3)_2N \rightarrow CH_2NCH_3 + H \quad (1)$$

$$(CH_3)_2N \rightarrow CH_2NH + CH_3 \quad (2)$$

Reaction 1 takes place in presence of an H scavenger, while reaction 2 has not yet been ascertained.[14]

Dubs et al.[15] performed two photon subdoppler laser induced fluorescence on the dissociation reaction of NDMA at 363.5 nm. Their results can be summarized as follows: (i) after fragmentation, the NO molecule retains 44.5% of the available energy, that is 18.4 kcal/mol, while dimethylamine radical bears the rest (23.0 kcal/mol); (ii) the experimental evidence is consistent with a fast dissociation process, which is short compared to a rotational period of the parent molecule but long relative to a vibrational period which implies the vibrational structure of the band; (iii) experimental facts are consistent with a planar dissociation.

In a series of works, Lavi et al.[16,17] studied the directional properties of the photodissociation processes after excitation onto the S_1 and S_2 states. Their findings are in good agreement with the previous results, although they affirm that the dissociation process after excitation at 363.5 deviates from planarity. In contrast, at 250 nm NDMA exhibits a planar character and is somewhat faster than the former. Additionally, the S_1 and S_2 states possess A' and A'' symmetry, respectively.

Theoretical studies on the photochemistry of this molecule are scarcer. Molecular dynamics calculations by Persico et al.[18a] on the S_1 ab initio potential-energy surface of NDMA also indicated the loss of planarity in the dissociation process in agreement with the experimental evidence of Lavi et al.[16,17] Cimaraglia et al.[18b] studied nitrosamine (NH_2NO) and they found that NH_2NO adopts a twisted and pyramidalized structure on S_1 without an exit barrier for the dissociation process. This result was also reproduced by our own CASPT2//CASSCF calculations on NH_2NO.[19]

In the present work, by means of the CASPT2//CASSCF methodology, we have studied the photochemistry of NDMA after excitation to S_2 and S_1 states respectively, as well as the ground-state unimolecular reactions of its photoproduct: dimethylamine radical (DMA). In section II, we introduce the methods of calculation; section III is divided in four parts, which, respectively present the analysis and discussion of the results on (a) the vertical transitions of NDMA, (b) the homolytic dissociation of NDMA after excitation to S_1 and S_2, (c) the

---

(8) *N-Nitrosodimethylamine*; Concise International Chemical Assessment Document No. 38; World Health Organization: Geneva, 2002.

(9) (a) Lazarou, Y. G.; Papagiannakopoulos, P. *J. Phys. Chem.* **1990**, *94*, 7114. (b) Nigenda, S. E.; McMillen, D. F.; Golden, D. M. *J. Phys. Chem.* **1989**, *93*, 1124.

(10) Diau, E. W.; Yu, T.; Wagner, M. A. G.; Lin, M. C. *J. Phys. Chem.* **1993**, *98*, 4034.

(11) (a) Plaksin, P. M.; Sharma, J.; Bulusu, S.; Adams, G. F. *J. Electron Spectrosc. Relat. Phenom.* **1975**, *6*, 429. (b) White, M. G.; Colton, R. J.; Lee, T. H.; Rabelais, J. W. *Chem. Phys.* **1975**, *8*, 391. (c) Kobayashi, T. *Z. Phys. Chem. Neue Folge* **1975**, *97*, 265.

(12) (a) Arenas, J. F.; Otero, J. C.; Peláez, D.; Soto, J. *J. Chem. Phys.* **2005**, *122*, 084324. (b) Arenas, J. F.; Otero, J. C.; Peláez, D.; Soto, J. *J. Phys. Chem. A* **2005**, *109*, 7172.

(13) (a) Chow, Y. L.; Wu, Z.-Z.; Lau, M.-P.; Yip, R. W. *J. Am. Chem. Soc.* **1985**, *107*, 8196. (b) Chow, Y. L. *Acc. Chem. Res.* **1973**, *6*, 354.

(14) (a) Geiger, G.; Huber, J. R. *Helv. Chim. Acta* **1981**, *64*, 989. (b) Geiger, G.; Stafast, H.; Brühlmann, U.; Huber, J. R. *Chem. Phys. Lett.* **1981**, *79*, 521.

(15) Dubs, M.; Brühlmann, U.; Huber, J. R. *J. Chem. Phys.* **1986**, *84*, 3106.

(16) (a) Lavi, R.; Bar, I.; Rosenwaks, S. *J. Chem. Phys.* **1987**, *86*, 1639. (b) Lavi, R.; Schwartz-Lavi, D.; Bar, I.; Rosenwaks, S. *J. Phys. Chem.* **1987**, *91*, 5398.

(17) Lavi, R.; Rosenwaks, S. *J. Chem. Phys.* **1988**, *89*, 1416.

(18) (a) Persico, M.; Cacelli, I.; Ferretti, A. *J. Chem. Phys.* **1991**, *94*, 5508. (b) Cimaraglia, R.; Persico, M.; Tomasi, J. *J. Am. Chem. Soc.* **1985**, *107*, 1617.

(19) Peláez, D.; Arenas, J. F.; Otero, J. C.; Soto, J. *J. Chem. Phys.* **2006**, *125*, 164311. (This paper, selected for the November **2006** issue of the *Virtual Journal of Ultrafast Science*.)

chemistry of the DMA fragment on the ground state, (d) the chemistry on the first excited triplet state, and (e) the possibility of tautomerizations. Section IV summarizes the main results and concludes the paper. For the sake of brevity, some Tables and Figures have been included in the Supporting Information.

II. Methods of Calculation

Throughout this work, we have made use of the CASPT2//CASSCF[20,21] methodology, both levels of calculation as implemented in the MOLCAS 6.4 quantum software package.[22] This protocol has been extensively proven to yield accurate and reliable results on the chemical behavior of many different systems.[12,19,23−28] All of the geometrical optimizations have been performed at the CASSCF/6-31G* level of calculation and the energy of all the critical and nonstationary points (Franck−Condon points and dissociation fragments at the asymptotic limit) have been recalculated at the CASPT2/CASSCF/ANO-L level. With respect to the atomic natural orbitals (ANO-L) basis sets,[29] the C, N, O [3s2p1d]/H [2s1p] contraction scheme is used. The use of a smaller basis set (6-31G*) for the geometrical optimizations is justified by the high-level calculations and by the large size of the molecule. However, the use of a more balanced basis set (ANO-L) for the recalculation of the energies ensures a quantitative description of the vertical transitions and relative energy of the excited potential-energy surfaces. Surface crossings, conical intersections, and intersystem crossings have been located with the Gaussian 03 set of programs.[30] To determine the relevant states in the NDMA photodecomposition, vertical transitions calculations have been performed (i) in gas phase and (ii) in solvent by means of the polarization continuum model (PCM) method.[31] The latter correspond to MS-CASPT2 single-point energy calculations at the ground-state minimum geometry using different solvents in increasing order of dielectric constant, namely, cyclohexane, benzene, methanol, and water.

All of the stationary points have been characterized by means of their harmonic vibrational CASSCF/6-31G* frequencies. Additionally, the characterization of the imaginary modes associated to the Franck−Condon geometries has been performed by computation of the CASSCF/ANO-L harmonic vibrational frequencies obtained from the mass-weighted Cartesian forces matrix, that is, Hessian matrix, after projecting out the contributions of the gradients, rotations, and translation, as described in a previous work.[32]

The analysis of the potential-energy surface between relevant points has been carried out by minimum energy path calculations (MEP) (or intrinsic reaction path calculations, when the starting point is a transition state) at the CASSCF level. In these calculations, we have made exclusive use of the ANO-L. To properly account for the dynamic electronic correlation along the paths, the energies of the optimized points along the reaction valley have been recomputed at the MS-CASPT2 level.

The topology of the potential-energy surfaces has been studied by performing linear interpolations in internal coordinates, as in previous works.[19,23−27] An interpolation vector, $\Delta\mathbf{R}$, which connects the geometries of the critical points of interest, for example, the geometries of stationary points and dissociation fragments, is obtained by calculating the difference between the internal coordinates of reactant and products, $\Delta\mathbf{R} = \mathbf{R}_p - \mathbf{R}_r$, where $\mathbf{R}_r$ and $\mathbf{R}_p$ represent the internal coordinate vectors of the reactants and products, respectively. Units of the interpolation vector are measured in Å for internuclear distances and degrees for valence and dihedral angles.

The interpolation vector is divided into a number of points which constitute intermediate geometries at which single point calculations are performed. These structures must be close enough to ensure a smooth convergence of the wavefunction. Thus, if the initial geometries are chosen carefully, these linear interpolations provide valuable information: (i) They constitute a good estimation of the reaction path; hence, they provide a good starting point for the location of a transition state. (ii) If an interpolation does not present an energy barrier, it implies that the actual minimum energy path lacks of transition state. (iii) When several electronic states are represented, surface crossings become evident. (iv) It is possible to study the variation of any property, such as fragment charge, along the interpolation.

The choice of the active space follows from our previous work on NH_2NO,[19] it involves 14 electrons distributed among 10 valence orbitals (Figure S1), namely,

$$2s_O, 2s_N, \sigma_{NN}, \pi_{NO}, \sigma_{NO}, np_N, np_O, \pi^*_{NO}, \sigma^*_{NN}, \sigma^*_{NO}$$

The study of the tautomerizations has been performed by taking into account a σ_{CH} orbital and its corresponding virtual orbital, so that the resulting active space spans 16 electrons distributed in 12 orbitals. The active space of the dimethylamine radical (DMA), which has been chosen in accordance with (i) H extrusion and (ii) methyl radical extrusion, includes the σ_{CN} orbitals, the corresponding σ_{CH} orbitals, the np_N, the $n\sigma_N$, and the corresponding virtuals, resulting in a CASSCF(11,10). The active space for the DMA fragments has been obtained by reduction of the former parent active space. With respect to the NO moiety, it has been optimized at the CASSCF(11,8) level, yielding an internuclear distance of 1.159 Å.

---

(20) (a) Andersson, K.; Malmqvist, P.-Å.; Roos, B. O.; Sadlej, A. J.; Wollinski, K. *J. Phys. Chem.* **1990**, *94*, 5483. (b) Andersson, K.; Malmqvist, P.-Å.; Roos, B. O. *J. Chem. Phys.* **1992**, *96*, 1218. (c) Finley, J.; Malmqvist, P.-Å.; Roos, B. O.; Serrano-Andrés, L. *Chem. Phys. Lett.* **1998**, *299*, 288.

(21) Roos, B. O. In *Advances in Chemical Physics; Ab Initio Methods in Quantum Chemistry;* Lawley, K. P., Ed.; Wiley: Chichester, U.K., 1987; Vol. II, Chapter 69, p 399.

(22) Karlström, G.; Lindh, R.; Malmqvist, P.-Å.; Roos, B. O.; Ryde, U.; Veryazov, V.; Widmark, P.-O.; Cossi, M.; Schimmelpfennig, B.; Neogrady, P.; Seijo, L. *Comput. Mater. Sci.* **2003**, *28*, 222.

(23) Arenas, J. F.; Otero, J. C.; Peláez, D.; Soto, J.; Serrano-Andrés, L. *J. Chem. Phys.* **2004**, *121*, 4127.

(24) Arenas, J. F.; Otero, J. C.; Peláez, D.; Soto, J. *J. Chem. Phys.* **2003**, *119*, 7814.

(25) Arenas, J. F.; Centeno, S. P.; López-Tocón, I.; Peláez, D.; Soto, J. *THEOCHEM* **2003**, *630*, 17.

(26) Arenas, J. F.; Otero, J. C.; Peláez, D.; Soto, J. *J. Org. Chem.* **2006**, *71*, 983.

(27) Soto, J.; Arenas, J. F.; Otero, J. C.; Peláez, D. *J. Phys. Chem. A* **2006**, *110*, 8221.

(28) Merchán, M.; González-Luque, R.; Climent, T.; Serrano-Andrés, L.; Rodríguez, E.; Reguero, M.; Peláez, D. *J. Phys. Chem. B* **2006**, *110*, 26471.

(29) Widmark, P.-O.; Malmqvist, P.-Å.; Roos, B. O. *Theor. Chim. Acta* **1990**, *77*, 291.

(30) Frisch, M. J.; Trucks, G. W.; Schlegel, H. B.; Scuseria, G. E.; Robb, M. A.; Cheeseman, J. R.; Montgomery, J. A., Jr.; Vreven, T.; Kudin, K. N.; Burant, J. C.; Millam, J. M.; Iyengar, S. S.; Tomasi, J.; Barone, V.; Mennucci, B.; Cossi, M.; Scalmani, G.; Rega, N.; Petersson, G. A.; Nakatsuji, H.; Hada, M.; Ehara, M.; Toyota, K.; Fukuda, R.; Hasegawa, J.; Ishida, M.; Nakajima, T.; Honda, Y.; Kitao, O.; Nakai, H.; Klene, M.; Li, X.; Knox, J. E.; Hratchian, H. P.; Cross, J. B.; Bakken, V.; Adamo, C.; Jaramillo, J.; Gomperts, R.; Stratmann, R. E.; Yazyev, O.; Austin, A. J.; Cammi, R.; Pomelli, C.; Ochterski, J. W.; Ayala, P. Y.; Morokuma, K.; Voth, G. A.; Salvador, P.; Dannenberg, J. J.; Zakrzewski, V. G.; Dapprich, S.; Daniels, A. D.; Strain, M. C.; Farkas, O.; Malick, D. K.; Rabuck, A. D.; Raghavachari, K.; Foresman, J. B.; Ortiz, J. V.; Cui, Q.; Baboul, A. G.; Clifford, S.; Cioslowski, J.; Stefanov, B. B.; Liu, G.; Liashenko, A.; Piskorz, P.; Komaromi, I.; Martin, R. L.; Fox, D. J.; Keith, T.; Al-Laham, M. A.; Peng, C. Y.; Nanayakkara, A.; Challacombe, M.; Gill, P. M. W.; Johnson, B.; Chen, W.; Wong, M. W.; Gonzalez, C.; Pople, J. A. *Gaussian 03*, revision B.04; Gaussian, Inc.: Wallingford, CT, 2004.

(31) Barone, V.; Cossi, M. *J. Phys. Chem. A* **1998**, *102*, 1995. (b) Cossi, M.; Rega, N.; Scalmani, G.; Barone, V. *J. Chem. Phys.* **2001**, *114*, 5691.

(32) Arenas, J. F.; Marcos, J. I.; López-Tocón, I.; Otero, J. C.; Soto, J. *J. Chem. Phys.* **2000**, *113*, 2282.

The CASPT2 calculations have been computed over a CASSCF reference wave function by leaving frozen the core orbitals ($1s_C$, $1s_N$, $1s_O$), that is, as optimized at the CASSCF level. To minimize the contamination of the perturbed wave function by intruder states as well as to ensure an acceptable weight of the CASSCF reference wave function, the technique of imaginary level shift[33] has been introduced as default in all the linear interpolations calculations. By doing this, we prevent situations in which the weight of the CASSCF wave function in the perturbative treatment becomes too low and, as a consequence, the CASPT2 potential-energy surface is not continuous. In such cases the CASPT2 treatment would lack significance.

The transition dipole moments were computed according to the CAS state interaction (CASSI) procedure[34] in conjunction with the perturbatively modified CAS (PMCAS-CI) reference functions obtained as linear combinations of all the states involved in the MS-CASPT2 calculation. The spin−orbit coupling constants, which are the matrix elements that represent the coupling between two states of different multiplicity, have been computed using an effective one-electron Fock-type spin−orbit Hamiltonian, as suggested by Hess and co-workers,[35] and with the RASSI program implemented in MOLCAS 6.4. To avoid the calculation of multicenter one- and two-electron integrals, the atomic mean field integrals (AMFI) have been used.[36] Spin−orbit coupling between configuration interaction (CI) eigenvectors of the effective Hamiltonian form a Hermitian matrix. Since the basis set is real and the spin−orbit operator is complex, all spin−orbit couplings are off-diagonal. The diagonal elements are the CI energies without spin−orbit couplings. Diagonalizing this Hermitian matrix yields spin−orbit coupled states.[37] To estimate the spin−orbit coupling interaction between two states of different multiplicity, we have used the root-mean-square formula defined in a previous work,[38a] which has been discussed and generalized in a recent work by Federov et al.[38b]

III. Results and Discussion

A. Ground-State Geometry and Vertical Transitions. The ground-state equilibrium geometry of NDMA has been studied at different levels of theory, namely, (i) CASSCF/6-31G*, (ii) CASSCF/ANO-L, (iii) CASPT2/ANO-L, (iv) B3LYP/6-31G*, and (v) B3LYP/cc-pVTZ. As observed in Table 1, the highest correlated methods (B3LYP and CASPT2), provide a planar C_2NNO frame, while both CASSCF calculations yield a slight deviation from planarity. Nevertheless, it is noted that the CASSCF/6-31G* set of parameters is in good agreement with the experimental values and, thus, will be used throughout this work. This choice responds to the need of a balance between computational cost and the reliability on the description of the electronic excited surfaces.

At this respect, the vertical transition calculations are not very sensitive to the choice of the ground-state geometry, as shown in Table 2. The first singlet excited state ($1^1A''$) occurs at 3.29 eV and possesses an $np_O \rightarrow \pi^*_{NO}$ character. The second excited singlet state ($2^1A'$) occurs at 5.30 eV and exhibits $np_N \rightarrow \pi^*_{NO}$ character. The corresponding oscillator strengths are 0.003 and 0.17, respectively. A change in the basis sets does not affect at all the oscillator strengths. Both sets of values are in good agreement with the experimental data.[14] For the sake of comparison, the vertical transitions at the C_s structure, optimized at the CASPT2/ANO-L level, have also been computed. Relative energies and oscillator strengths agree with the MS-CASPT2/ANO-L values at the CASSCF/6-31G* geometry.

TABLE 1. Selected Geometrical Parameters of NDMA Ground-State Minimum Geometry at Different Levels of Calculation

	CASSCF		CASPT2	DFT		
parameter[a,b]	6-31G*	ANO-L	ANO-L	6-31G*	ccpVTZ	exptl[c]
$R_{2,1}$	1.368	1.368	1.355	1.337	1.336	1.329
$R_{3,2}$	1.227	1.222	1.241	1.230	1.217	1.233
$R_{4,1}$	1.444	1.447	1.454	1.456	1.451	1.448
$R_{5,1}$	1.441	1.444	1.451	1.450	1.445	1.448
$R_{6,4}$	1.081	1.087	1.097	1.095	1.086	
$R_{7,5}$	1.080	1.086	1.099	1.092	1.087	
$R_{8,4}$	1.081	1.086	1.101	1.091	1.092	
$R_{9,5}$	1.084	1.089	1.108	1.097	1.093	
$A_{3,2,1}$	114.4	114.7	115.4	114.1	116.5	114.0
$A_{4,1,2}$	120.3	120.4	123.3	120.3	123.2	
$A_{5,1,4}$	122.5	121.7	120.7	122.8	120.6	122.5
$A_{6,4,1}$	110.1	110.1	107.6	110.3	107.8	
$A_{7,5,1}$	108.1	108.2	107.6	107.2	107.8	
$A_{8,4,1}$	108.5	108.2	109.8	108.6	110.3	
$A_{9,5,1}$	110.5	110.2	110.5	111.1	110.9	
$Dh_{4,1,2,3}$	-4.6	-6.4	0.0	0.0	0.0	
$Dh_{5,1,2,3}$	-171.6	-169.5	180.	179.8	180.0	
$Dh_{6,4,1,2}$	53.3	53.3	0.0	-0.2	0.0	
$Dh_{7,5,1,2}$	-12.1	-14.7	0.0	0.1	0.0	

[a] Atom labeling according to Figure 1a. [b] *R*, internuclear distances in Å; *A* (Dh), valence (dihedral) angles in degrees. [c] Experimental values from ref 4.

TABLE 2. MS-CASPT2 Energies of the Vertical Transitions of NDMA to the Lowest Energy Singlet and Triplet States

state	configuration	weight[a]	$\Delta E^{b,c}$	$f^{\,d}$	ΔE_{exp}	f_{exp}
$1^1A'$	G.S.	0.91	0.00			
$1^1A''$	$np_O \rightarrow \pi^*_{NO}$	0.92	3.29	0.003	3.41[e]	0.009[e]
			(3.32)	(0.003)		
			[3.34]	[0.003]		
$2^1A'$	$np_N \rightarrow \pi^*_{NO}$	0.83	5.30	0.17	5.46[e]	0.12[e]
			(5.54)	(0.17)		
			[5.21]	[0.18]		
$3^1A''$	$\sigma_{NO} \rightarrow \pi^*_{NO}$	0.50	7.51	0.006		
	$np_N \rightarrow \pi^*_{NO}$	0.25	(7.57)	(0.006)		
			[7.41]	[0.006]		
$1^3A''$	$np_O \rightarrow \pi^*_{NO}$	0.93	2.48		2.73 [f]	
			(2.50)			
			[2.59]			
$1^3A'$	$np_N \rightarrow \pi^*_{NO}$	0.94	3.80			
			(3.93)			
			[3.72]			

[a] Weight of the configuration on the MS-CASPT2 wave function. [b] MS-CASPT2/ANO-L energy difference in eV, reference energy = −263.78538 hartrees. In parentheses, MS-CASPT2/6-31G* energy difference in eV, reference energy = −263.65245 hartrees. Singlet states are averaged to four states, triplet states are averaged to two states. [c] In brackets, MS-CASPT2/ANO-L energy difference in eV for the CASPT2 ground-state minimum of C_s symmetry. Reference energy = −263.78577 hartrees. Singlet states of each symmetry are averaged to three states. [d] MS-CASPT2/ANO-L oscillator strength in atomic units. In parentheses, MS-CASPT2/6-31G* values; in brackets, MS-CASPT2/ANO-L values of the oscillator strengths for the CASPT2 ground-state minimum of C_s geometry. [e] Experimental values from ref 14a. [f] Energy of the $S_0 \rightarrow T_1$ transition from ref 13a.

Chow and co-workers[13] showed that the band corresponding to the $S_0 \rightarrow T_1$ transition appeared at 453 nm (2.73 eV) in methylcyclohexane solution. In addition, the band center exhibited a blue-shift as the solvent polarity was increased. To analyze this feature, we have performed polarization continuum

---

(33) Forsberg, N.; Malmqvist, P.-Å. *Chem. Phys. Lett.* **1997**, *274*, 196.

(34) Malmqvist, P.-Å. *Int. J. Quantum Chem.* **1986**, *30*, 470.

(35) Hess, B. A.; Marian, C.; Wahlgren, U.; Gropen, O. *Chem. Phys. Lett.* **1996**, *265*, 965.

(36) Malmqvist, P.-Å.; Roos, B. O.; Schimmelpfenning, B. *Chem. Phys. Lett.* **2002**, *357*, 230.

(37) Ribbing, C.; Gilliams, B.; Pierloot, K.; Roos, B. O.; Karlström, G. J. *Chem. Phys.* **1998**, *109*, 3145.

(38) (a) Furlani, T. R.; King, H. F. *J. Chem. Phys.* **1985**, *82*, 5577. (b) Federov, D. G.; Koseki, S.; Schmidt, M. W.; Gordon, M. S. *Int. Rev. Phys. Chem.* **2003**, *22*, 551.

TABLE 3. PCM MS-CASPT2 Energies of the Vertical Transitions of NDMA to the Lowest Energy Singlet and Triplet States

	gas phase[b]		cyclohexane[b]		benzene[b]		methanol[b]		water[b]	
state[a]	Δ*E*	*f*	Δ*E*	*f*	Δ*E*	*f*	Δ*E*	*f*	Δ*E*	*f*
$1^1A'$	0.00		0.00		0.00		0.00		0.00	
$1^1A''$	3.29	0.321×10^{-2}	3.30	0.322×10^{-2}	3.31	0.323×10^{-2}	3.34	0.327×10^{-2}	3.34	0.327×10^{-2}
$2^1A'$	5.30	0.172	5.25	0.175	5.26	0.176	5.24	0.181	5.24	0.181
$3^1A''$	7.51	0.567×10^{-2}	7.53	0.557×10^{-2}	7.53	0.555×10^{-2}	7.58	0.534×10^{-2}	7.56	0.532×10^{-2}
$1^3A''$	2.48		2.54		2.55		2.63		2.64	
$1^3A'$	3.80		3.68		3.66		3.47		3.46	

[a] Vertical transitions labeled in C_s symmetry. [b] Energy differences in eV and oscillator strengths in atomic units. Reference MS-CASPT2/ANO-L energy: (i) gas phase, −263.78538 hartrees; (ii) cyclohexane, −263.78840 hartrees; (iii) benzene, −263.78881 hartrees; (iv) methanol, −263.79316 hartrees; (v) water, −263.79341 hartrees.

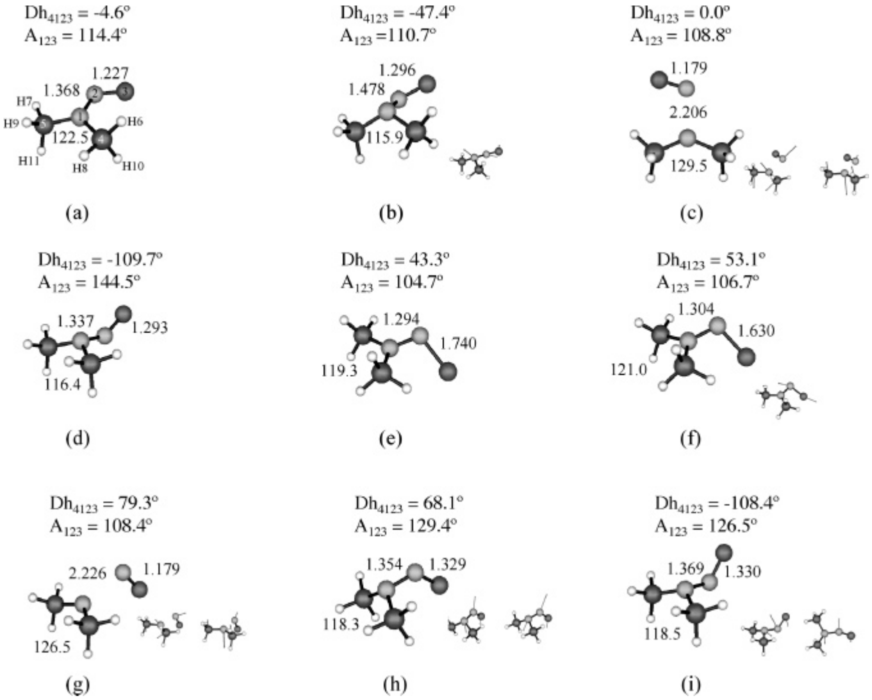

FIGURE 1. Critical points of NDMA of relevance in its decomposition after excitation to the S_1 and S_2 surfaces. The arrows in the smaller figures correspond to (i) stationary points, imaginary modes; (ii) conical intersections, gradient difference and non-adiabatic coupling vectors: (a) S_0 minimum (Ml); (b) S_1 transition state for the N−N bond cleavage (Sd1); (c) S_2/S_1 conical intersection (Ci1); (d) S_2 minimum (M2); (e) S_2 minimum (M3); (f) S_2 first-order saddle point (Sd2); (g) S_2/S_1 conical intersection (Ci1b); (h) S_3/S_2 conical intersection (Ci2); (i) S_3/S_2 conical intersection (Ci3).

model (PCM) calculations for various solvents in increasing order of polarity, namely, cyclohexane, benzene, methanol, and water. The results are collected in Table 3. These single point PCM/MS-CASPT2 calculations reproduce the observed effect: the first triplet transition shifts from 2.48 eV in gas phase to 2.64 eV in water. With respect to the singlet−singlet transitions, the lowest energy band is blue-shifted as solvent polarity increases, and the high-energy one is red-shifted. However, both shifts are small. The oscillator strengths for the former band remain essentially unaltered while those for the latter undergo a slight increase.

The vertical transition calculations have provided the nature of the electronic states involved in the photodecomposition process. In the following sections, such mechanism will be analyzed. First, the relevant critical points, in each case, will be introduced. Then, the corresponding potential-energy surfaces will be studied by means of linear interpolations in internal coordinates, and/or minimum energy paths calculations. Finally, all this information, (i) character of the critical point, (ii) relative energies, and (iii) topology of the potential-energy surface, will allow us to establish a coherent picture of NDMA reactivity.

B. Dissociation of NDMA after Irradiation at 363.5 and 248 nm. With respect to the N−N homolytic dissociation of NDMA, the following critical points have been located: (i) an S_0 minimum (M1) (Figure 1a); (ii) a first-order saddle point corresponding to the transition state for the homolytic dissociation on S_1 (Figure 1b); (iii) an S_2/S_1 conical intersection (Ci1) (Figure 1c); (iv) an S_2 minimum (M2) (Figure 1d); (v) an S_2 minimum (M3) (Figure 1e); (vi) an S_2 first-order saddle point (Sd2) (Figure 1f); (vii) an S_2/S_1 conical intersection (Ci1b) (Figure 1g). Finally, two S_3/S_2 conical intersections (Ci2 and Ci3) are the only critical points found on the S_3 surface (Figure 1h,i). Their relative energies, referred to the ground-state minimum energy, are collected in Table S2.

In Figure S2a (Supporting Information), the C_1 energy profile for the homolytic dissociation into $(CH_3)_2N$ (1^2B_1) + NO $(X^2\Pi)$ on the four lowest singlet surfaces is presented. On S_0, it corresponds to a path without exit barrier, as it is common to other related molecules.[12,19,23−27] It is noteworthy that all electronic transitions at the dissociation limit take place on the DMA fragment. As a consequence, given the degenerated nature of the electronic ground state of NO $(X^2\Pi)$, both sets of states

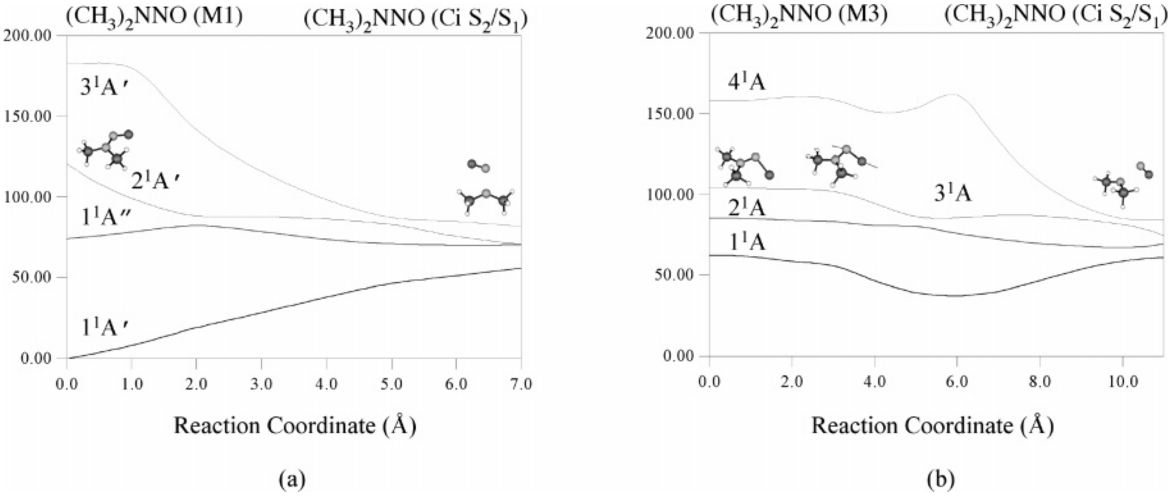

FIGURE 2. MS-CASPT2 energy profiles for the MEP optimized points along the reaction paths connecting (a) Franck−Condon geometry and the S_2/S_1 conical intersection Ci1 and (b) S_2 minimum (M3) and the S_2/S_1 conical intersection Ci1b through Sd2. Initial and final geometries are labeled on top of the vertical axis together with a pictorial representation of the geometry. Character of the states is indicated at the beginning of the curves.

(S_0 and S_1) and (S_2 and S_3) converge in turn at that limit. The CASPT2/ANO-L asymptotic energy for the first two singlet states is 48.6 kcal/mol over the ground-state minimum geometry.

According to the vertical transitions, the S_1 Franck−Condon point occurs at 75.9 kcal/mol (3.29 eV) over M1. This surface possesses a dissociative character; in fact, the only stationary point on this surface, Sd1, corresponds to the transition state for the N−N homolytic dissociation. This result agrees with the available experimental data[17] and previous theoretical works.[18a,19] Figure S2b reproduces the potential-energy curves of C_1 symmetry connecting Sd1 and the dissociation products, $(CH_3)_2N$ (1^2B_1) + NO ($X^2\Pi$), on the four lowest singlet surfaces.

The reactivity of NDMA on the S_2 surface is controlled by the occurrence of the S_2/S_1 conical intersection, Ci1. This planar critical point exhibits an internuclear N−N distance of 2.206 Å, and both gradient difference and nonadiabatic coupling vectors point toward dissociation, as shown in Figure 1c. Both vectors define the resulting momenta after the internal conversion process, as discussed in previous works.[12a] An MS-CASPT2/ANO-L linear interpolation of C_s symmetry between the Franck−Condon geometry (optimized C_s) and Ci1 reveals that both points are connected trough a barrierless path (Figure S2c). To confirm the existence of the correspodent reaction path, a CASSCF/ANO-L MEP calculation was performed. For such calculation, an initial geometry must be obtained by a slight distortion of the reference geometry (Franck−Condon point) in the direction of the imaginary mode associated to its highest frequency vibration. These frequencies are obtained after projection of the Hessian matrix, as described in the Methods of Calculation section. In Figure 2a, we present the MS-CASPT2/ANO-L energy curves for the points optimized along the reaction path; it can be observed that they lead directly to the S_2/S_1 conical intersection (Ci1). Consequently, the most probable route after excitation to the S_2 state would be the decay through an S_2/S_1 planar conical intersection in accordance to the experimental results of Dubs et al.[15] and in analogy with our previous results on NH_2NO.[19] Therefore, the photoproducts are generated in their ground electronic state, that is $(CH_3)_2N$ (1^2B_1) + NO ($X^2\Pi$). For the sake of comparison, all of the CASSCF/ANO-L MEP curves have been included in Figure S3. In the following paragraphs, minor competing channels will be considered.

Adiabatic dissociation on S_2 surface yields $(CH_3)_2N$ (1^2A_1) and NO ($X^2\Pi$). Nevertheless, as it will be demonstrated in the next section, the first excited doublet state of $(CH_3)_2N$ (1^2A_1) leads directly to an D_1/D_0 conical intersection ($1^2A_1/1^2B_1$) analogously to NH_2 (1^2A_1).[19] Hence, the only photoproduct would be $(CH_3)_2N$ (1^2B_1). Dissociation from the Franck−Condon geometry into $(CH_3)_2N$ (D_1/D_0) + NO ($X^2\Pi$) has been studied by means of a linear interpolation in internal coordinates (Figure S2 d). From this calculation, an upper limit can be estimated of 13.4 kcal/mol over M2 to the energy barrier of such a process. Therefore, it is clear that excitation to S_2 (122.2 kcal/mol) provides enough energy to NDMA to proceed through this dissociative channel. Additionally, other stationary points occur on the S_2 surface: two minima, M2 and M3, and a first-order saddle point, Sd2. This point constitutes the CASSCF/6-31G* transition state connecting the minimum M3 to an S_2/S_1 conical intersection, Cib. It is interesting that the small CASSCF/6-31G* energy difference between M3 and Sd2, below 1 kcal/mol, remains at the CASSCF/ANO-L level: 1.1 kcal/mol, (Table S2). However, it reverses sign when dynamic correlation energy is included: (i) −2.4 kcal/mol at the CASPT2/6-31G* level and (ii) −2 kcal/mol at the CASPT2/ANO-L level (Table S2). These results are illustrated in the minimum energy paths calculations. The CASSCF/ANO-L MEP calculation shows an energy barrier (Figure S3b). On the other hand, the CASPT2 potential-energy curve obtained from the MEP optimized points consists of a barrierless path (Figure 2b).

Summarizing, photodissociation of NDMA, independently of the excitation energy, implies the N−N bond breaking through two main different mechanisms: (i) barrierless decomposition from a twisted transition state on S_1 or (ii) after excitation to S_2, initial deactivation through the planar S_2/S_1 conical intersection (Ci1), and dissociation on S_1. Therefore, the photoproducts are in both cases the same: $(CH_3)_2N$ (1^2B_1) and NO ($X^2\Pi$).

C. Ground-State Chemistry of the Dimethylamine Fragment. Experimentally, it is observed that irradiation at 363.5 nm ($S_0 \rightarrow S_1$) implies initial NDMA decomposition into $(CH_3)_2N$ + NO followed by association of the fragments (long-lived DMA radical and NO) to yield the initial product with a

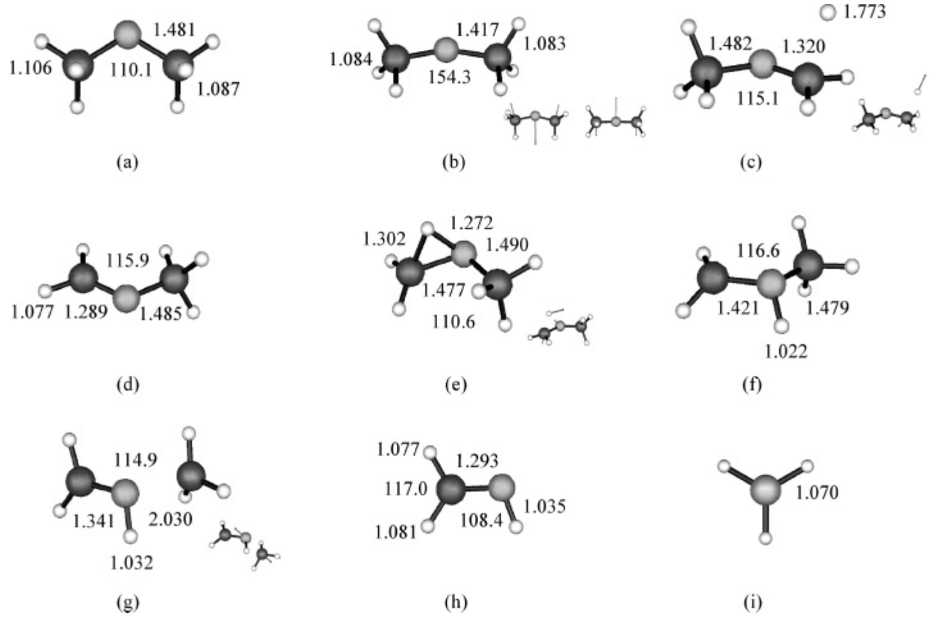

FIGURE 3. Relevant critical points of DMA and derivatives related to NDMA photodissociation. The arrows in the smaller figures correspond to (i) stationary points, imaginary modes; (ii) conical intersection, gradient difference and nonadiabatic coupling vectors: (a) $(CH_3)_2N$ (1^2B_1) minimum (M_{DMA}); (b) D_1/D_0 conical intersection (Ci_{DMA}); (c) transition state for the H extrusion (Ts_H); (d) *N*-methylidene-methylamine minimum; (e) transition state for the 1,2-H migration ($Ts_{1,2H}$); (f) CH_2NHCH_3 intermediate minimum; (g) transition state for the methyl radical extrusion Ts_{CH3}; (h) methylidene-methylimine minimum; (i) methyl radical.

quantum yield of unity.[14] On the contrary, irradiation at 248 nm ($S_0 \rightarrow S_2$) gives a totally different picture because of the reactivity of the DMA radical. In this case, a wide manifold of photoproducts are generated. However, in the last section the proposed mechanism indicates that the same photoproducts are generated in both cases. Therefore, to describe properly this differential photochemistry not only topological considerations must be taken into account but also dynamical data such as the energy distribution of the fragments. Hence, to complement our results, we will refer to the experimental energy distributions obtained by Dubs et al.[15]

In Figure 3 the geometries of all the critical points involved in the DMA chemistry as well as those of the relevant fragments are presented, namely, (i) ground-state minimum, M_{DMA} (Figure 3a), (ii) D_1/D_0 conical intersection, CI_{DMA} (Figure 3b), (iii) transition state for the hydrogen abstraction, Ts_H (Figure 3c), (iv) minimum *N*-methylidene-methylamine, (CH_2NCH_3) (Figure 3d), (v) transition state for the 1,2-H migration, $Ts_{1,2H}$ (Figure 3e), (vi) intermediate minimum CH_2NHCH_3 (Figure 3f), (vii) transition state for the methyl radical extrusion, Ts_{CH3} (Figure 3g), (viii) methylidene-imine minimum (CH_2NH) (Figure 3h), and (ix) methyl radical (Figure 3i). The relative energies, referred to M_{DMA}, are collected in Table S3.

At the experimental wavelengths, DMA can be formed in two different electronic states: the ground state D_0 (1^2B_1) and the first excited doublet state D_1 (1^2A_1). As stated in the previous section, the D_1 surface lacks of minimum, in fact the lowest energy point on this surface corresponds to an D_1/D_0 conical intersection (Ci_{DMA}) (Figure 3b), at 40.2 kcal/mol over M_{DMA}. The path connecting the Franck−Condon geometry of DMA and the conical intersection is barrierless for both D_0 and D_1, as shown by the MS-CASPT2/ANO-L linear interpolation in Figure 4a. Hence, if DMA is generated in its first excited singlet state (1^2A_1), the most likely process is the deactivation through the D_1/D_0 conical intersection (Ci_{DMA}). Both gradient difference and nonadiabatic coupling vectors point to the region of M_{DMA}, as a consequence the final product would be DMA in its ground electronic state, 1^2B_1.

At the level of calculation used in this work, we have been able to identify channels (1) and (2). The reaction of hydrogen abstraction (1) (feasible in the presence of an H scavenger) is a one-step process, which proceeds through the transition state Ts_H at 41.3 kcal/mol over M_{DMA} at the CASPT2 level. The potential-energy curve connecting M_{DMA} and the dissociation products, $CH_2NCH_3 + H$, passing through Ts_H is presented in Figure 4b. On the other hand, methyl radical extrusion (2) consists of two steps: (i) 1,2-H migration to the N to form CH_2NHCH_3 through $Ts_{1,2H}$ and (ii) extrusion of methyl radical through Ts_{CH3} to yield $CH_2NH + CH_3$. The energy barriers are: 44.0 kcal/mol ($Ts_{1,2H}$) and 31.5 kcal/mol (Ts_{CH3}), respectively. These relative energies indicate an effective competition of both processes, path (1) being slightly favored. The CASPT2 linear interpolation for reaction (2) is displayed in Figure 4c.

The energy distributions obtained by Dubs, Brühlmann and Huber for the dissociation of NDMA after irradiation at 363.5 nm,[15] indicate that the total available energy for the DMA fragment, including electronic, vibrational, and rotational contributions, amounts up to 23.0 kcal/mol, consequently the dissociation of NDMA on S_1 does not provide enough energy to the DMA fragment to surmount the barriers corresponding to channels (1) or (2). This fact is in agreement with the long-lived DMA radical and the subsequent recombination of DMA and NO to reform NDMA. On the other hand, decomposition of NDMA starting at S_2 implies a totally different mechanism because of a different topology of the potential-energy surface along the reaction path and an extra available energy, over 46 kcal/mol, to be distributed between DMA and NO. In this case, without dynamical calculations, out of the scope of this work, the distribution of the available energy between the fragments cannot be inferred. However, the experimental data suggest that this higher available energy is distributed in such a way that

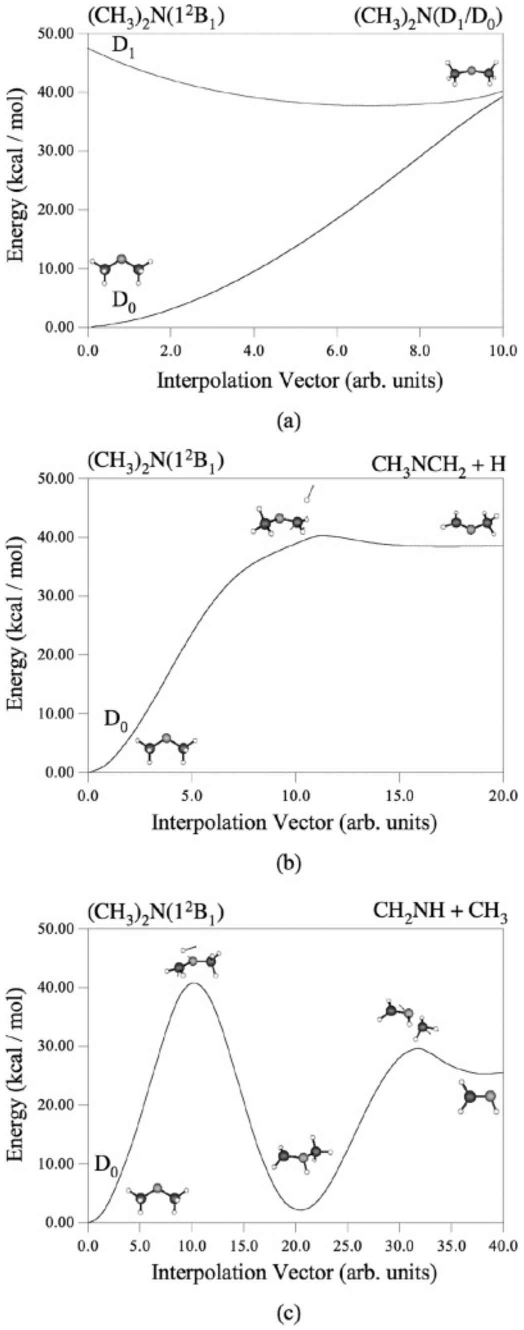

FIGURE 4. MS-CASPT2 linear interpolations for the reaction paths of DMA connecting (a) M_{DMA} and Ci_{DMA}; (b) M_{DMA} and the dissociation products CH_3NCH_2 + H through the transition state Ts_H; (c) M_{DMA} and the dissociation products $CH_2NH + CH_3$ in two steps: (1) initial 1,2-H migration through $Ts_{1,2H}$ to yield intermediate CH_3NHCH_2 and (2) decomposition of the intermediate through Ts_{CH3}. Initial and final geometries are represented on top of the vertical axis. Electronic state is indicated at the beginning of the curves.

DMA results with enough energy to surmount the barriers and reacts according to channels (1) and (2).

D. Phosphorescence and the Chemistry of NDMA on the T_1 Surface. The experimental results by Chow and co-workers[13a] indicate that the $S_0 \rightarrow T_1$ excitation of NDMA in EPA glass at 77 K by irradiation at 440 nm is possible. This result has motivated our study of the T_1 electronic state. The phosphorescence emission spectrum exhibits a band which peaks approximately at 530 nm (54 kcal/mol) and a shoulder centered around 560 nm (51 kcal/mol).

On the first triplet state surface, the following critical points have been found: (i) T_1/S_0 intersystem crossing (Isc1) (Figure 5a), (ii) minimum (M4) (Figure 5b), (iii) minimum (M5) (Figure 5 (c), (iv) transition state for the dissociation on T_1 (Sd3) (Figure 5d), (v) T_1/S_0 intersystem crossing (Isc2) (Figure 5e), (vi) nitrene minimum (M6) (Figure 5f), and (vii) transition state for the dissociation of M6 on T_1 (Sd4) (Figure 5g). The relative energies of all these points, referred to M1, are collected in Table S4.

MS-CASPT2/ANO-L vertical-transition calculations show that the T_1 surface occurs at 2.48 eV (57.2 kcal/mol). Additionally, in the region of the Franck−Condon point, two minima, M4 and M5, have been located. Several facts indicate that these two points may be responsible for the phosphorescence emission: (i) the small energy difference between the peaks in the phosphorescence emission spectrum (∼3 kcal/mol) is noticeable; (ii) the relative energies of M4 and M3, referred to ground-state minimum (M1), are, respectively, 51.3 kcal/mol and 49.8 kcal/mol including ZPE corrections; (iii) their geometries are close to the ground-state geometry; (iv) their computed spin−orbit coupling constants are 72.8 and 73.4 cm^{-1}, respectively.

With respect to the T_1 reactivity, the transition state for the homolytic dissociation on this surface (Sd3) occurs at 3.1 kcal/mol over M5, that is, after excitation from S_0, the adiabatic dissociation is energetically allowed. The linear interpolations in internal coordinates corresponding to the intersystem crossing Isc1 and dissociation from M5 are displayed in Figure S4 parts a and b, respectively.

Finally, a brief remark has to be made on the nitrene isomer. We have studied its decomposition into $(CH_3)_2N$ + NO on the lowest singlet and triplet surfaces by means of MS-CASPT2/ANO-L linear interpolations. Our results indicate that singlet surfaces are purely dissociative in this region, as shown in Figure S4c. On the other hand, the first triplet surface presents a transition state for the homolytic dissociation, Sd4. At the CASSCF level this point is just 1.2 kcal/mol over nitrene minimum M6, while the CASPT2 linear interpolations yield an upper limit of 7.2 kcal/mol.

E. Tautomerizations of NDMA. In this last section, we consider the possibility of H migration from the methyl moieties to the N, O atoms of the nitroso group, analogously to NH_2-NO.[19] Our aim is to determine whether these processes may participate in the global reaction or their contribution can be neglected instead. The calculation and comparison of the energy barriers for the corresponding transition states constitute a good estimation of their relative meaning.

In relation to tautomerizations, the following relevant stationary points have been located: (i) minimum NDMA, M1 (Figure S5a), (ii) transition state for the H migration to the nitroso O (Ts_{OH}) (Figure S5b), (iii) minimum (M_{OH}) (Figure S5c), (iv) transition state for the H migration to the nitroso N (Ts_{NHO}) (Figure S5d), (v) minimum (M_{NHO}) (Figure S5e), (vi) transition state for the $M_{OH} \leftrightarrow M_{NHO}$ isomerization (Ts_{OH-HNO}) (Figure S5f). Attached to each figure, the CASPT2 relative energies of all these points are displayed.

The energy barriers for the Ts_{OH} and Ts_{NHO} transition states are 36.9 kcal/mol and 65.4 kcal/mol, respectively. Consequently, the former may compete with the homolytic dissociation on the ground state. Additionally, direct $M_{OH} \rightarrow M_{HNO}$ isomerization is hindered by the high-energy barrier of the Ts_{OH-HNO} transition

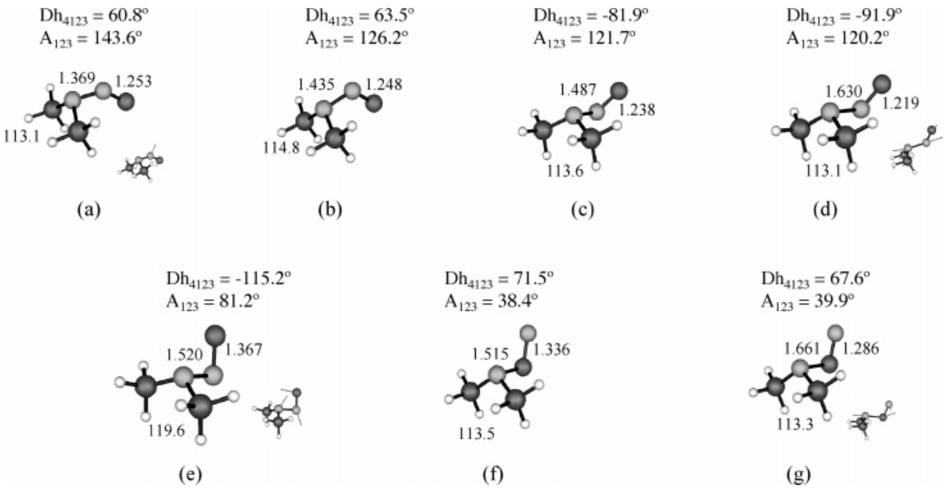

FIGURE 5. Relevant critical points of NDMA on the T_1 surface. The arrows in the smaller figures correspond to (i) stationary points, imaginary modes; (ii) intersystem crossings, gradient difference vectors: (a) T_1/S_0 intersystem crossing (Isc1); (b) T_1 minimum (M4); (c) T_1 minimum (M5); (d) transition state for the N−N homolytic dissociation on T_1 (Sd3); (e) T_1/S_0 intersystem crossing (Isc2); (f) T_1 nitrene minimum (M6); (g) transition state for the N−N homolytic dissociation of nitrene on T_1 (Sd4).

state: 80.7 kcal/mol. Hence, the only possibility is the formation of M_{OH}. The meaningfulness of this isomer lies in the fact that its decomposition would yield CH_3NCH_2 and NOH, the former species being one of the photoproducts of the decomposition of NDMA: *N*-methylidene-methylamine. Hence, this route may constitute another source of this product. This decomposition can take place either adiabatically, that is on the singlet surface (higher energy path) or on the triplet surface (lower energy path) after an S_0/T_1 intersystem crossing. However, these two paths can be neglected. Several facts support this: (i) the reverse tautomerization to M1 is by far the lowest energy process, 10.3 kcal/mol from M_{OH}; (ii) the transition state for the adiabatic decomposition occurs at a high energy, a CASPT2 linear interpolation yields an upper limit of 74.5 kcal/mol relative to M_{OH}; (iii) the intersystem crossing is prevented because of its extremely low value of the spin−orbit coupling constant, just 4.3 cm^{-1}, and its relative energy 31.2 kcal/mol over M_{OH}. Consequently, no contribution to the global process can be expected from tautomerizations.

IV. Conclusions

The decomposition mechanisms of NDMA after excitation to S_1 or S_2 have been studied by means of the CASPT2//CASSCF methodology. The global reaction depends on the available energy for DMA after NDMA fragmentation. Dissociation on both states yields the same photoproducts: $(CH_3)_2N$ (1^2B_1) + NO (X^2P). However, if reaction starts on S_1, the resulting DMA fragment does not possess enough energy to surmount the barriers leading to (a) H abstraction, a one-step process (41.3 kcal/mol) or (b) methyl radical extrusion, a two-step reaction consisting of (1) an initial 1,2-H migration to form the intermediate CH_2NHCH_3 (44.0 kcal/mol) followed by (2) methyl extrusion (31.5 kcal/mol). This fact implies a long-lived radical which recombines with NO to reform NDMA and, as a consequence, no global reaction is observed. On the contrary, dissociation starting at S_2, provides the system with a relative energy excess of 46 kcal/mol which is sufficient for DMA reactions to take place and to generate the secondary products, *N*-methylidene-methylamine (CH_3NCH_2) and methylidene-imine (CH_2NH).

With respect to the first excited triplet state, the occurrence of two minima which correlate in their relative energy to the values of the two peaks in the observed phosphorescence emission band have been shown. Moreover, the spin−orbit coupling constants indicate a high probability of emission from these two points. Additionally, dissociation on this surface is a low cost process (3.1 kcal/mol) and thus likely to occur.

Finally, the possibility of tautomerization has been considered. The relative energy of the respective transition states suggest that these paths are forbidden and do not compete with homolytic dissociation.

Acknowledgment. This research has been supported by the Spanish Ministerio de Educación y Ciencia (Project BQU2003-1426). Daniel Peláez thanks the Spanish Ministerio de Educación y Ciencia for the Grant BES-2004-6033.

Supporting Information Available: Table showing the following: atom coordinates in SI units (pm) for all the presented geometries; the energies of the relevant critical points in the NDMA photochemistry after excitation at S_1 and S_2 states; the energies of the relevant critical points related to DMA reactivity; the energies of the relevant critical points of NDMA on the first triplet surface. Figures displaying the following: the orbitals included in the NDMA active space; MS-CASPT2 energy profiles of the main dissociation channels of NDMA on the first four singlet states; CASSCF/ANO-L MEP energy profiles of the relevant paths on the S_2 surface; MS-CASPT2 linear interpolations related to the main paths on the T_1 surface; comparison of the relevant tautomerization paths of NDMA. This material is available free of charge via the Internet at http://pubs.acs.org.

JO070399A